catalysts

MDPI

Perspective

Porphyrins Acting as Photosensitizers in the Photocatalytic CO_2 Reduction Reaction

Yusuke Kuramochi * and Akiharu Satake *

Department of Chemistry, Faculty of Science Division II, Tokyo University of Science, Tokyo 162-8601, Japan
* Correspondence: kuramochiy@rs.tus.ac.jp (Y.K.); asatake@rs.tus.ac.jp (A.S.)

Abstract: The success of the photocatalytic CO_2 reduction using sunlight depends on how visible light is captured and utilized. Zn porphyrins, which are synthetic analogues of chlorophyll and bacteriochlorophyll, have very intense absorption bands in the visible region and are high potential candidates as photosensitizers for CO_2 reduction. However, the use of zinc porphyrins had been limited due to their poor stability under the photocatalytic reduction conditions. We found that the durability of porphyrin during the photocatalytic CO_2 reduction reaction is dramatically improved by combining a metal complex catalyst with the porphyrin so that two or more electrons are not accumulated on the porphyrin. In this perspective, we describe the molecular design of systems that combine Re complexes and porphyrins in detail and their unique reaction mechanisms in the photocatalytic CO_2 reduction.

Keywords: porphyrin; CO_2 reduction; photosensitizer; photocatalyst

1. Introduction

The increase in atmospheric CO_2 has caused serious environmental problems, such as global warming and ocean acidification. Global CO_2 emissions from fossil fuels and industry continue to increase, reaching 37.1 billion tons in 2021 [1]. Humans obtain energy by burning fossil fuels, and CO_2 is released during the oxidation reaction process. Therefore, to store energy in CO_2 and to utilize it as a carbon source, a reduction reaction of CO_2 is required. However, because CO_2 is the most oxidized and stable state of carbon, the equilibrium potential of the one-electron reduction of CO_2 is very high at −1.9 V versus the standard hydrogen electrode (SHE) at pH 7 aqueous solution (Equation (1)). On the other hand, CO_2 reduction reactions involving multiple electrons can be used at much more positive potentials than that of the one-electron reduction. For instance, the equilibrium potentials of two-electron reductions of CO_2 are −0.52 and −0.61 V vs. SHE at pH 7 for CO and formic acid, respectively (Equations (2) and (3)) [2]. Another problem that must be solved for CO_2 reduction is competitive hydrogen evolution by proton reduction. The equilibrium potential of hydrogen evolution is more positive (−0.42 V vs. SHE at pH 7; Equation (4)) than those of two-electron reductions of CO_2, indicating that hydrogen evolution is a thermodynamically favorable process. Therefore, a catalyst that not only drives the multielectron reduction reaction but also suppresses hydrogen evolution is essential.

Metal complexes are promising candidates as CO_2 reduction catalysts because metal complexes can have multiple accessible redox states and high activation energy against proton reduction [2–10]. In addition, their catalytic properties and the reaction sites can be designed at the molecular level through the selection of an appropriate metal and ligands. Most of the metal complexes yield CO and/or HCOOH as the two-electron reduction products of CO_2, whereas some complexes produce oxalate (oxalic acid) [11] and methane [12]. Re(I) diimine carbonyl complexes are advantageous as catalysts for CO_2 reduction because the Re complexes almost exclusively provide CO without the formations of HCOOH and H_2, even in aqueous solutions. Since the Re complexes have absorption in

check for updates

Citation: Kuramochi, Y.; Satake, A. Porphyrins Acting as Photosensitizers in the Photocatalytic CO_2 Reduction Reaction. *Catalysts* **2023**, *13*, 282. https://doi.org/10.3390/catal13020282

Academic Editor: Fernando Fresno

Received: 24 December 2022
Revised: 21 January 2023
Accepted: 25 January 2023
Published: 27 January 2023

the near-UV to visible region, they also act as photosensitizers in the photocatalytic CO_2 reduction reaction, but their durability is low. On the other hand, it has been reported that combining the Re complex with an appropriate photosensitizer, i.e., Ru(II) trisdiimine complex, dramatically improves the efficiency and durability of the photocatalytic CO_2 reduction [2].

$$CO_2 + e^- \rightarrow CO_2^{\bullet -}: -1.9 \text{ V } \textit{vs. SHE (at pH 7)} \quad (1)$$

$$CO_2 + 2H^+ + 2e^- \rightarrow CO + H_2O: -0.52 \text{ V} \quad (2)$$

$$CO_2 + 2H^+ + 2e^- \rightarrow HCOOH: -0.61 \text{ V} \quad (3)$$

$$2H^+ + 2e^- \rightarrow H_2: -0.42 \text{ V} \quad (4)$$

Hybrid systems of a semiconductor and metal complex, which can extract electrons from water and reduce CO_2 selectively, have been developed [13–15]. To achieve both the oxidation of water and the reduction of CO_2 using visible light, a two-stage and double-excitation process is required. Ishitani and coworkers utilized a dinuclear Ru(II)–Re(I) complex as the reduction site of an artificial Z-scheme photocatalyst, where the Ru and Re complexes act as a photosensitizer and a catalyst, respectively (Figure 1) [14,16]. Visible light irradiation of the Ru–Re complex immobilized on a semiconductor-catalyzed selective CO_2 reduction to give CO using electrons that were supplied from the visible-light-driven semiconductor for water oxidation with high efficiency and selectivity. The Ru–Re complex has already been investigated in detail in the presence of sacrificial reducing reagents, such as 1-benzyl-1,4-dihydronicotinamide and 1,3-dimethyl-2-phenyl-2,3-dihydro-1*H*-benzo[d]imidazole (BIH), and has been shown to have high catalytic activity for the photocatalytic CO_2 reduction [17]. When BIH was used as the electron donor in *N*,*N*-dimethylformamide (DMF) and triethanolamine (TEOA), the turnover number (TON_{CO}) and reaction quantum yield (Φ_{CO}) for the photocatalytic CO_2 reduction reached more than 3000 and 45%, respectively [18]. In homogeneous reactions, the catalyst can be evaluated directly without considering the combination with the oxidation site, and it is relatively easy to investigate the reaction mechanisms using spectroscopic techniques. Various catalysts, photosensitizers, electron donors, solvents, and catalytic properties used in homogeneous catalytic systems are not described in detail. Interested readers are directed to some previous reviews [2–5,8,10]. Although the Ru–Re complex showed high activity and durability for the photocatalytic CO_2 reduction, the absorption ability of the Ru trisdiimine complex is not sufficient for fully utilizing sunlight on the semiconductors. Thus, the accumulation of photosensitizers [19] and/or the development of photosensitizers that more strongly absorb visible light are required. This perspective focuses on porphyrins, one of the organic compounds with the highest ability to absorb visible-light, and describes systems combining porphyrin with the Re complex catalysts for the CO_2 reduction.

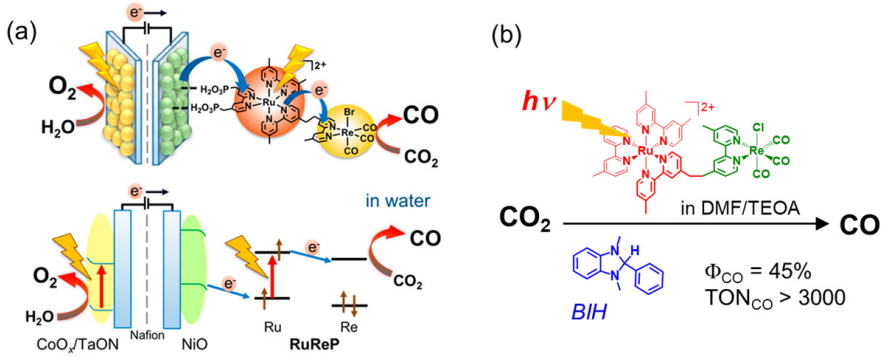

Figure 1. (**a**) An artificial Z-scheme photocatalyst combining semiconductors and a Ru–Re complex for photocatalytic CO_2 reduction using water as an electron donor. Adapted with permission from [16]. Copyright 2019 American Chemical Society. (**b**) A photocatalyst evaluation system for the Ru–Re complex using a sacrificial reducing reagent [18].

2. Dyad Systems Based on a Porphyrin–Re Complex

Zn(II) porphyrins are widely used instead of magnesium tetrapyrrole compounds as synthetic analogues and model molecules for chlorophylls (Chls) and bacteriochlorophylls (BChls) (Mg complexes) [20–24]. Magnesium porphyrins are highly sensitive toward acid, and the demetallation of the magnesium ion easily occurs even in silica gel columns [25]. Free-base and Zn porphyrins have intense absorption bands in the visible region and can retain the singlet excited states that exhibit fluorescence, allowing the long-range singlet–singlet energy transfer, as observed in the Chls and BChls of photosynthetic systems [20]. Here, Zn(II) has a closed-shell d^{10} configuration and does not give low-energy states that facilitate the thermal deactivation of the excited energy. On the other hand, for instance, a Ni(II) porphyrin, which has a d^8 configuration, gives a metastable dd excited state in <20 ps and returns to the ground state in approximately 200 ps [26]. Porphyrins have been utilized as photosensitizers in photocatalytic CO_2 reduction systems [27]. Among them, several dyads composed of a porphyrin and a Re complex catalyst have been studied using sacrificial electron donors in homogeneous systems, and Zn porphyrins tend to show higher performance (Figure 2) [28–34]. Although various metal complexes have been developed as the reduction catalyst [2–10], to our knowledge, there have been no dyad systems so far that combine a porphyrin as the photosensitizer and a metal complex other than the Re complex as the catalyst for CO_2 reduction.

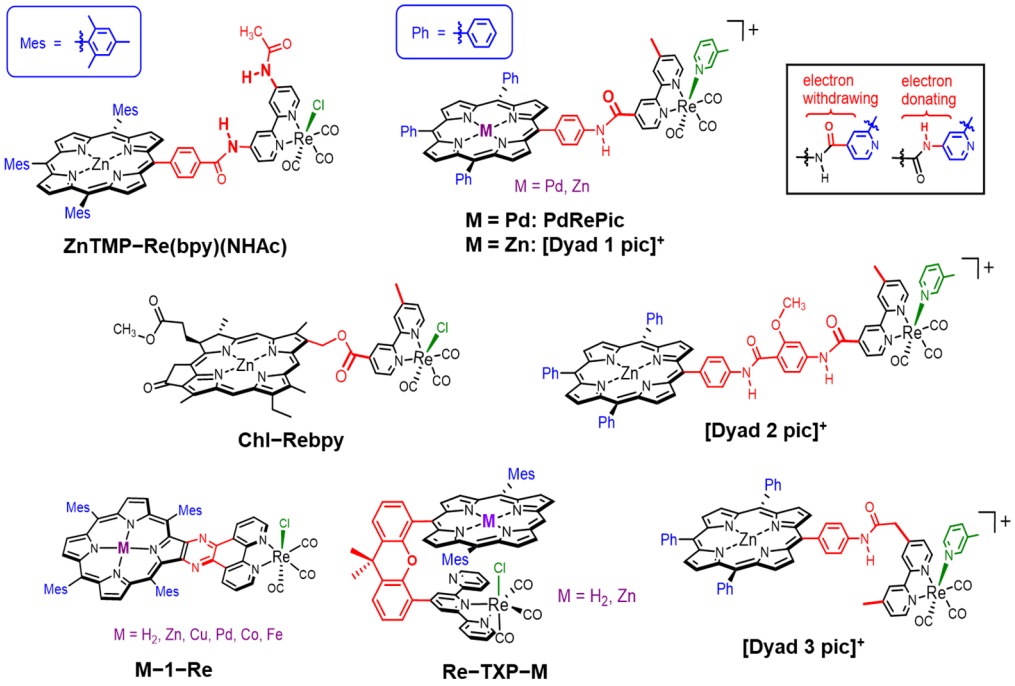

Figure 2. Molecular structures of the porphyrin (chlorin)–Re complex dyads for photocatalytic CO_2 reduction. When the carbamoyl substituent is attached to the bpy ligand through a C=O or N–H moiety, the substituent acts as a weak electron-withdrawing or -donating group for the bpy ligand, respectively [35].

Inoue et al. reported the photocatalytic CO_2 reduction reaction using a Zn porphyrin linked with a Re complex via a phenyl carbamoyl moiety (**ZnTMP–Re(bpy)(NHAc)**) [28]. The Zn porphyrin has mesityl groups at *meso*-positions and the Re complex has an acylamide substituent on the 2,2′-bipyridine (bpy) ligand in addition to the bridging amide. In this dyad, the N–H moiety of the carbamoyl is linked to the bpy ligand. Excitation at 428 nm to **ZnTMP–Re(bpy)(NHAc)** in the presence of triethylamine (TEA) as an electron donor gave the reduction product whose reaction quantum yield was 0.64% and the TON was not described. In **ZnTMP–Re(bpy)(NHAc)**, excitation to the second excited singlet state (S_2) of the porphyrin induced the intramolecular electron transfer from the Zn porphyrin to the

Re complex but the lifetime of the charge-separated (CS) state was short (90 ps). The lowest excited state (S_1) of the porphyrin did not cause the intramolecular electron transfer but an internal conversion and intersystem crossing to the first excited triplet state (T_1).

Perutz et al. reported a dyad consisting of a palladium(II) porphyrin as the photosensitizer and the Re complex via an acylanilide moiety (**PdRePic**) [29]. In this dyad, the acylanilide moiety is substituted as a carbamoyl group with the bpy ligand. The Pd porphyrin exhibited room temperature phosphorescence accompanied by weak fluorescence when excited at 522 nm in degassed butyronitrile [36]. The irradiation at >420 nm of DMF and TEA solutions containing **PdRePic** gave CO, whose TON_{CO} was 2 after 4 h. A rather high TON_{CO} of 3 was obtained after 4 h in the mixed system of the Pd porphyrin and Re complex units, and an induction period of the CO formation indicated that the catalytic active photosensitizer was a Pd chlorin species, which was obtained by the hydrogenation of the Pd porphyrin.

The same group also reported dyads composed of Zn porphyrin and Re complex via two kinds of amide linkers (**[Dyad 1 pic]$^+$** and **[Dyad 2 pic]$^+$**) [30]. **[Dyad 1 pic]$^+$** has the same structure as **PdRePic** except that the central part of the porphyrin is changed from Pd to Zn. In **[Dyad 2 pic]$^+$**, the porphyrin moiety and the Re complex are linked via a longer linker, a bisacylanilide group. Photophysical properties of **[Dyad 1 pic]$^+$** have been investigated in detail with time-resolved spectroscopic measurements [37]. In **[Dyad 1 pic]$^+$**, the intramolecular electron transfer from the excited S_1 state of the Zn porphyrin to the Re complex gave the CS state, but the rapid back-electron transfer occurred in tens of picoseconds (55 ps) [37]. The photocatalytic CO_2 reductions were carried out using two dyads in DMF and TEOA as the electron donor under irradiation at >520 nm. However, although the activity of **[Dyad 2 pic]$^+$** was higher than that of **[Dyad 1 pic]$^+$**, the catalytic activities of the dyads were lower than that of the mixed system of Zn tetraphenylporphyrin (ZnTPP) and the corresponding Re complex (TON_{CO} = 103 after 220 min for the mixed system). During photoirradiation in the presence of TEOA, the porphyrin of the dyad was hydrogenated to chlorin and finally bleached. In the case of Zn porphyrins, the Zn chlorin species acts as a poorer photosensitizer than the Zn porphyrin [30].

Perutz et al. also demonstrated that the dyad (**[Dyad 3 pic]$^+$**), in which the Zn porphyrin and the Re complex are linked via an extended acylanilide moiety with a methylene group, dramatically improved the photocatalytic activity of the CO_2 reduction reaction [31]. By introducing the methylene group, the reduction potential of **[Dyad 3 pic]$^+$** was significantly shifted to the negative side (−1.68 V vs. Fc/Fc^+) compared with the previous two dyads (−1.44 V and −1.42 V vs. Fc/Fc^+ for **[Dyad 1 pic]$^+$** and **[Dyad 2 pic]$^+$**, respectively). In **[Dyad 3 pic]$^+$**, the fluorescence of the Zn porphyrin was quenched by 23% in CH_2Cl_2, whereas the quenching extents of **[Dyad 1 pic]$^+$** and **[Dyad 2 pic]$^+$** were 95% and 55%, respectively. The fluorescence quenching resulted from the intramolecular electron transfer from the S_1 of porphyrin to the Re complex upon the excitation of the porphyrin. Among the three dyads, **[Dyad 3 pic]$^+$** had the longest lifetime of the CS state (320 ps). The photocatalytic CO_2 reduction using **[Dyad 3 pic]$^+$** in DMF/TEOA under irradiation at >520 nm gave CO, whose TON_{CO} reached 360. This value is one order magnitude larger than those ($TON_{CO} \approx 30$) of **[Dyad 1 pic]$^+$** and **[Dyad 2 pic]$^+$**. However, even in this case, the irradiation induced the hydrogenation of the porphyrin to give chlorin and isobacteriochlorin species, which were further hydrogenated and eventually bleached.

In **[Dyad 1 pic]$^+$** and **[Dyad 2 pic]$^+$**, the bpy ligands are substituted with the linker groups in a carbamoyl manner. In the carbamoyl-type substitution, the bpy ligand is affected by the substituent as a weak electron-withdrawing group. The reduction potential of the metal bpy carbonyl complex having weakly electron-deficient bpy shifts to the positive side, resulting in the potential change significantly decreasing the photocatalytic activity [35]. The Re bpy tricarbonyl complex having strongly withdrawing CF_3 groups becomes almost completely inactive for photocatalytic CO_2 reduction [38]. The high activity of **[Dyad 3 pic]$^+$** could be significantly attributed to the enhanced reactivity on the Re complex by changing the electronic properties.

Tamiaki et al. used chlorin as the photosensitizer (**Chl–Rebpy**) [32]. The introduction of the Re complex quenched the fluorescence of the chlorin in DMF, suggesting that the intramolecular electron transfer from the S_1 of chlorin to the Re complex occurred. The photocatalytic CO_2 reduction in DMF/TEOA using BIH as the photosensitizer gave CO, whose TON_{CO} was 18.

Tschierlei and Schwalbe et al. investigated the photocatalytic CO_2 reductions of phenanthroline (phen)-extended porphyrin series, in which the phen coordinated a Re tricarbonyl complex (**M-1–Re**) and the porphyrin is conjugated with the Re complex [33]. Although several dyads with Cu, Pd, Zn, Co, and Fe porphyrins were prepared, only the Zn porphyrin dyad (**Zn-1–Re**) gave sufficient amounts of CO (TON_{CO} = 12.8 after 24 h) in a CO_2-saturated DMF/TEA solution under irradiation at >375 nm. Other dyads gave no or trace amounts of CO (TON_{CO} < 1).

The same group reported the photocatalytic CO_2 reduction using hetero-Pacman dyads where a Re terpyridine complex is linked with a cofacially aligned free-base or Zn porphyrin via a xanthene moiety (**Re–TXP–M**) [34]. The crystal structure revealed that only two pyridines of the terpyridine unit coordinated to the Re ion in **Re–TXP–M**. The electronic interactions between the porphyrin and the Re complex were weak in the ground state, and the fluorescence intensities of the free-base and Zn porphyrin (**Re–TXP–H_2** and **Re–TXP–Zn**) were decreased by the introduction of the Re complex in CH_2Cl_2. The photocatalytic CO_2 reductions were carried out using two kinds of electron donors, TEA and BIH/TEOA. Irradiation at >450 nm for 24 h gave TON_{CO} = 6.1 for **Re–TXP–Zn** and no CO formation for **Re–TXP–H_2** when TEA was used. In contrast, the use of BIH/TEOA instead of TEA significantly promoted the catalytic reaction, resulting in TON_{CO} = 195 for **Re–TXP–Zn** and 13 for **Re–TXP–H_2**. Here, BIH has a stronger reductive power (E_{ox} = +0.33 V vs. saturated calomel electrode (SCE)) than TEA (E_{ox}~+0.96 V vs. SCE) [2]. The central metal ion of the porphyrin significantly contributed to the catalytic activity as observed in **M-1–Re**. In addition, the TON_{CO} of **Re–TXP–Zn** was one order of magnitude larger than that of the mixed system of the corresponding Zn porphyrin and Re complex (TON_{CO} = 22), showing the advantage of the dyad system.

3. Behavior of Electrochemical Reduction of Zn Porphyrin

In the dyad systems, Zn porphyrin shows a high photosensitizing ability in the photocatalytic CO_2 reduction. However, Perutz et al. reported that Zn porphyrins were hydrogenated at the C=C bonds of the porphyrin skeleton during the photocatalytic reaction. The UV–vis absorption spectral change in **[Dyad 3 pic]$^+$** showed that the Q bands of the Zn porphyrin decreased accompanied by a growing band at 625 nm, corresponding to chlorin species followed by isobacteriochlorin species at 620 nm at early irradiation time. As the irradiation continued, the Q bands were eventually bleached (Figure 3) [30,31]. Noting that the CO_2 reduction requires multielectron reduction, it is inevitable that more than two electrons accumulate in the catalyst, causing the hydrogenation of the porphyrin.

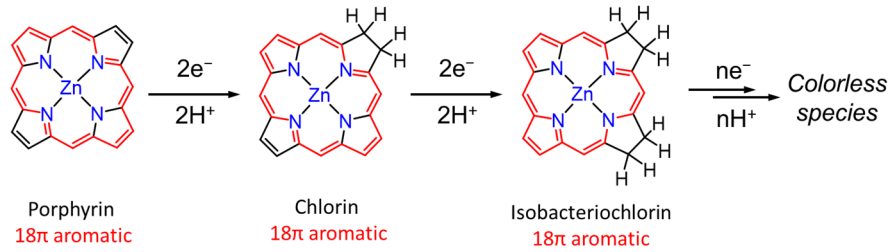

Figure 3. A decomposition process of Zn porphyrin during the photoreduction reaction [31].

The reduction behavior of Zn porphyrin (ZnTPP) has been investigated in detail by electrochemical reduction reactions (Figures 4 and 5). In the first and second reductions of Zn porphyrin, the valence of the central Zn ion is unchanged, and the reduction reactions basically occur on the π-conjugated porphyrin skeleton. The cyclic voltammetry of ZnTPP

in DMF showed that the first reduction wave at −1.3 V was reversible, indicating that the one-electron reduced species (OERS) of ZnTPP is stable (Figure 4) [39,40]. In contrast, the second reduction wave at −1.7 V became irreversible at a slower scan rate, and a new anodic peak at −0.5 V appeared. The new peak corresponds to the oxidation of the phlorin anion formed by protonation of the two-electron-reduced species of ZnTPP. The phlorin anion is a protonated species at the *meso*-position of the two-electron-reduced porphyrin. The OERS of ZnTPP and the phlorin anion show characteristic broad absorption bands at 710 and 825 nm, respectively (Figure 4). The phlorin anion is oxidized and deprotonated to the original ZnTPP. The phlorin anion is less stable and is also converted by protonation into a stable chlorin [41,42]. Electrochemical measurements demonstrated that while the two-electron-reduced species of Zn porphyrin is readily converted to Zn phlorin followed by Zn chlorin, the OERS of Zn porphyrin is stable. Thus, we considered that the suppression of the two-electron accumulation on Zn porphyrin by transferring the electron to the Re complex would lead to a highly durable photocatalyst.

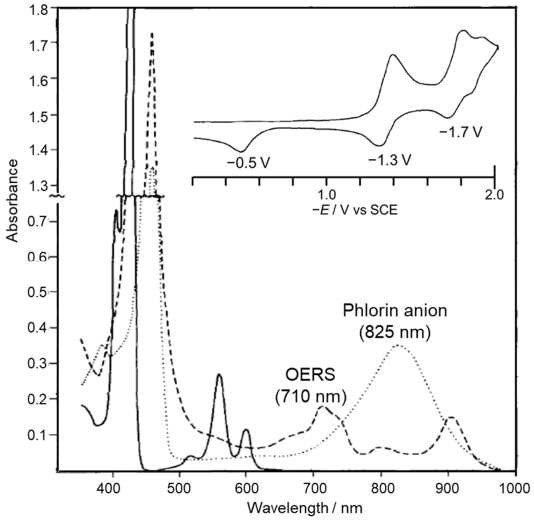

Figure 4. UV–vis absorption spectra of ZnTPP (solid line) and the reduction products (OERS: broken line, and phlorin anion: dotted line) in DMF-containing electrolytes in thin layer cell. Inset shows CV of ZnTPP (Scan rate: 0.033 V s^{-1}). Concentration: 1.5 × 10^{-3} M ZnTPP. Adapted with permission from [39] (partially modified). © The Electrochemical Society. Reproduced by permission of IOP Publishing. All rights reserved.

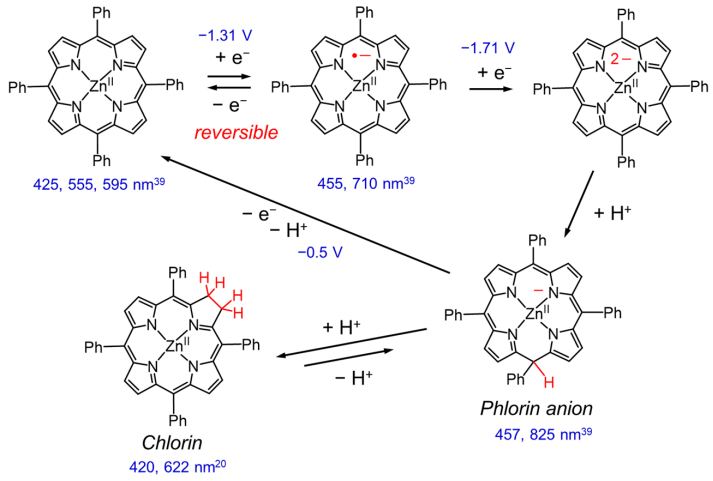

Figure 5. Electrochemical reduction of ZnTPP [39] and formation of chlorin [41,42]. The redox potentials are denoted with respect to an aqueous SCE [39]. The numbers in nm are peak wavelengths of UV–vis absorption spectra.

4. Porphyrin–Re Complex Dyads with Direct and Orthogonal Connection

We designed the porphyrin–Re complex dyads in which a Re phen tricarbonyl complex was directly connected with a free-base or Zn porphyrin at the *meso*-position of the porphyrin (**MP-phen=Re** in Figure 6) [43,44]. It is noteworthy that the phen ligand and the porphyrin ring are oriented orthogonally and each Re complex and porphyrin unit are not conjugated. In **MP-phen=Re**, it is expected that the rapid electron transfer of the reduced porphyrin to the Re complex prevents electron accumulation on the porphyrin part. Figure 7 shows the UV–vis absorption spectra of **ZnP-phen=Re**, **ZnP-phen** and **H_2P-phen=Re** compared with that of a widely used Ru complex ($[Ru(dmb)_3]^{2+}$; dmb = 4,4′-dimethyl-2,2′-bipyridine). The absorption coefficients of the Soret bands for **ZnP-phen=Re**, **ZnP-phen,** and **H_2P-phen=Re** ($\varepsilon > 200{,}000\ M^{-1}\ cm^{-1}$) are more than one magnitude larger than that of $[Ru(dmb)_3]^{2+}$ ($\varepsilon \approx 15{,}000\ M^{-1}\ cm^{-1}$). In addition, the porphyrins have relatively intense Q bands at more than 540 nm ($\varepsilon > 15{,}000\ M^{-1}\ cm^{-1}$), whereas $[Ru(dmb)_3]^{2+}$ has almost no absorption bands. The broader Soret band of **ZnP-phen=Re** than **ZnP-phen** indicates a strong electronic interaction between the Zn porphyrin and the Re complex. A similar broadening was observed in **H_2P-phen=Re**.

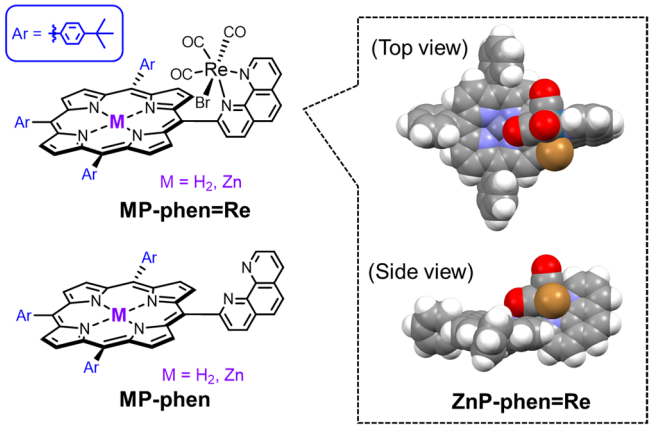

Figure 6. (**Left**) Chemical structures of the porphyrin–Re complex dyads with direct and orthogonal binding (**MP-phen=Re**) and the corresponding porphyrins (**MP-phen**). (**Right**) Molecular model of **ZnP-phen=Re** optimized using a density functional theory calculation [43,44].

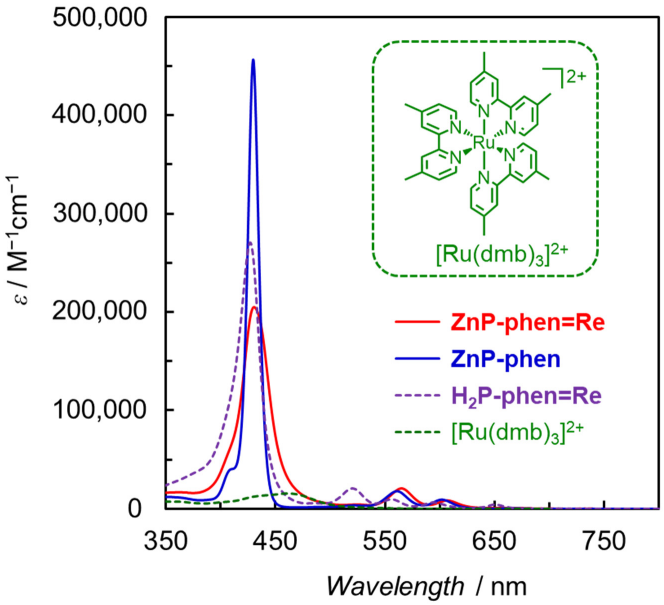

Figure 7. UV–vis absorption spectra of **ZnP-phen=Re, ZnP-phen,** and **H_2P-phen=Re** with $[Ru(dmb)_3]^{2+}$ [43,44].

The strong electronic interactions observed in the UV–vis absorption spectra also affected the emission spectra. The fluorescence of the free-base and Zn porphyrins was almost completely quenched by the introduction of the Re complex. Considering that the fluorescence quenching occurs even in **H_2P-phen=Re**, in which the intramolecular electron transfer from the S_1 of porphyrin to the Re complex is thermodynamically very unfavorable, the quenching was induced by a rapid intersystem crossing caused by the heavy Re atom. Surprisingly, the emission spectrum of **ZnP-phen=Re** measured in carefully degassed *N*,*N*-dimethylacetamide (DMA) under Ar showed weak but distinct room temperature phosphorescence of Zn porphyrin at ca. 800 nm (Figure 8) [43]. Herein, DMA is a solvent practically used for the photocatalytic CO_2 reduction [45]. Phosphorescence of Zn porphyrin is generally not observed at room temperature, but the heavy atom effect of Re would induce a unique room temperature phosphorescence. In contrast, **H_2P-phen=Re** did not show room temperature phosphorescence under the same conditions, probably because free-base porphyrin has a much lower phosphorescent ability than Zn porphyrin [44,46]. The phosphorescence of the Zn porphyrin was efficiently quenched by the electron donor, BIH, whereas the fluorescence at 610 and 660 nm was hardly quenched. This reflects that the intermolecular electron transfer with BIH more efficiently proceeds with the long-lived T_1 than the short-lived S_1 of porphyrin. The efficient phosphorescence quenching indicates that the quantitative photoinduced electron transfer occurs from BIH to the T_1 of **ZnP-phen=Re**.

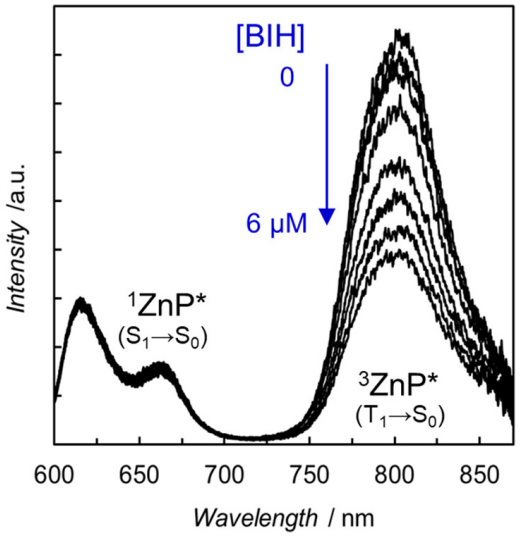

Figure 8. Emission spectra of **ZnP-phen=Re** in the presence of various amounts of BIH. Excited at 560 nm in Ar-saturated DMA at 298 K [43].

Photocatalytic CO_2 reductions using **ZnP-phen=Re** and **H_2P-phen=Re** were carried out in DMA-containing BIH as the electron donor under irradiation at 420 nm (without phenol (PhOH) in Figure 9a) [44]. The dyads gave CO with high selectivity (>99.9%) without forming formic acid and hydrogen. In the mixed system of ZnTPP and the corresponding Re complex as a control experiment, the color of the initial solution suddenly faded because of the decomposition of ZnTPP at the commencement of the irradiation, and the reaction was stopped ($TON_{CO} \approx 6$). This would result from the electron accumulation of ZnTPP, causing the bleaching. The TON_{CO} for **ZnP-phen=Re** reached more than 500, whereas the TON_{CO} for **H_2P-phen=Re** resulted in a lower value (<200). The electrochemical measurements showed that the Re complex part was more readily reduced than the Zn porphyrin part in **ZnP-phen=Re**, whereas in **H_2P-phen=Re**, the free-base porphyrin was more readily reduced, indicating that the OERS localizes the electron on the free-base porphyrin part. This difference in electrochemical structure would lead to a difference in the photocatalytic durability.

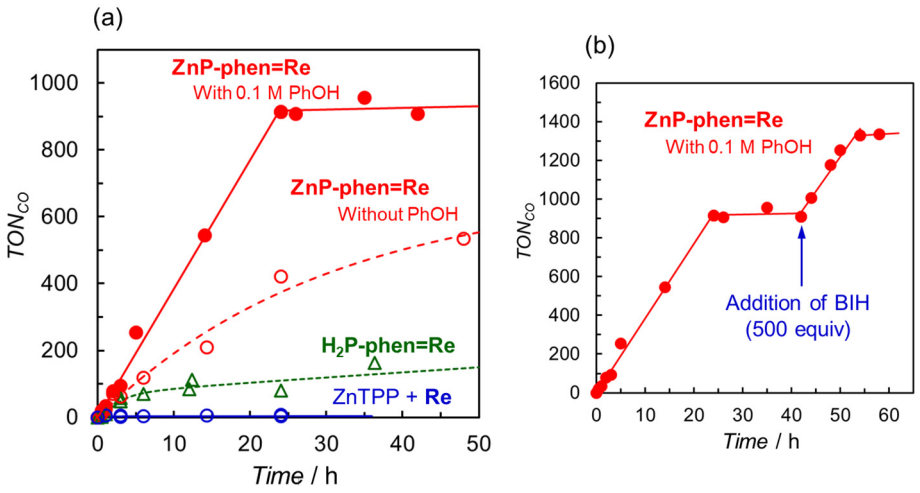

Figure 9. (**a**) Time dependences of CO formation during irradiation at 420 nm in CO_2-saturated DMA solutions containing BIH (1000 equiv against the Re complex) in the presence of **ZnP-phen=Re** with (red filled circle) and without PhOH (red open circle), **H_2P-phen=Re** (green open triangle), and a mixed system of ZnTPP and *fac*-Re(phen)$(CO)_3$Br (**Re**) (blue open circle). (**b**) Further addition of BIH to **ZnP-phen=Re** after 42 h of irradiation in the presence of PhOH [43,44].

PhOH is reported to be a proton source that can promote the CO_2 reduction reaction on the Re complex [47], suppressing the electron accumulation in **ZnP-phen=Re**. The addition of PhOH enhanced the rate of CO production for **ZnP-phen=Re** (red filled circle in Figure 9a). The enhancement by PhOH was not observed in **H_2P-phen=Re**. The TON_{CO} of **ZnP-phen=Re** reached more than 900, corresponding to an almost quantitative amount of added BIH (1000 equiv against the Re complex) and further addition of 500 equiv of BIH to the reaction mixture restarted the photocatalytic system with the same reaction rate (Figure 9b). The TON_{CO} finally reached more than 1300. In addition, the rate of CO production remained constant like a zero-order reaction until BIH was completely consumed. It was considered that the electron transfer from BIH through the long-lived T_1 of the Zn porphyrin proceeded efficiently, even if the concentration of BIH became lowered. This process was also supported by the energy diagram that was estimated from the photo- and electrochemical measurements (Figure 10). These results indicated that **ZnP-phen=Re** showed very high durability for the photocatalytic CO_2 reduction, which is attributed to the neighboring Re complex part, which acts as an electron reservoir to suppress electron accumulation on the porphyrin. The reaction proceeded similarly by exciting the Q band of the zinc porphyrin with 560 nm light. The reaction quantum yields for the CO formation were estimated using weak light upon excitation to the S_2 (λ_{ex} = 420 nm) and the S_1 (λ_{ex} = 560 nm) to be the same high values of 8%, indicating no deactivation process from the S_2 to the S_1. The dyad of **ZnP-phen=Re** achieved not only high durability but also high reaction efficiency.

We also carried out the photocatalytic CO_2 reduction using **ZnP-phen=Re** with TEA as the electron donor (Figure 11a) [44]. The TON_{CO} for **ZnP-phen=Re** reached a value of 23 after 60 h and the CO production continued even after 60 h. Although the CO formation was selectively observed, the TON_{CO} was an order of magnitude lower than that using BIH. However, the value of TON_{CO} > 25 was the highest in the reported dyads composed of a porphyrin and a Re complex in close proximity. The UV–vis absorption spectral change during irradiation showed the formation of Zn chlorin species at early irradiation time (Figure 11b). The time profile with an inflection point at ca. 10 h indicated that the formed Zn chlorin continued the catalytic reaction despite a lower activity of the chlorin than the porphyrin in **ZnP-phen=Re**. In contrast, the reaction solutions of **H_2P-phen=Re** and the mixed system were bleached, and the reactions were terminated after 10 h. The effect of the proton source was also examined in the reaction using **ZnP-phen=Re** and BIH, showing that trifluoroethanol also enhanced the catalytic reaction. The addition of acetic

acid caused a rapid bleaching of the porphyrin, suggesting that the formation of the Re hydride complex induces the hydrogenation of the porphyrin skeleton instead of hydrogen or formic acid production.

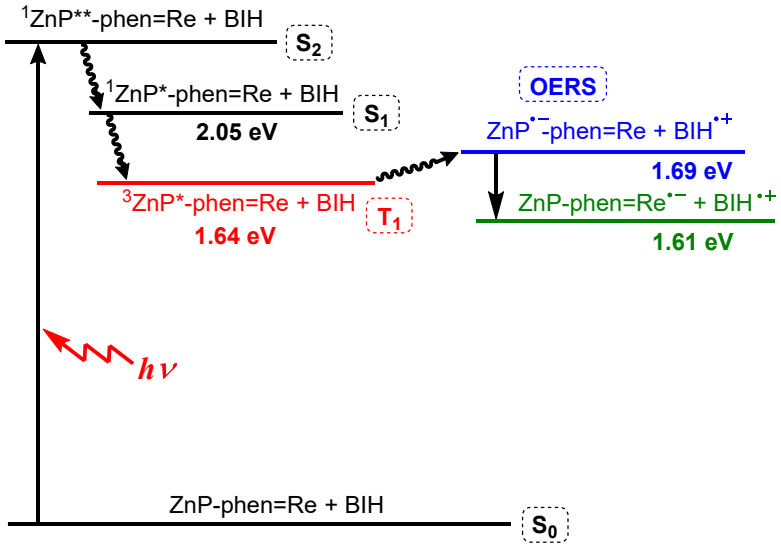

Figure 10. Energy diagram of **ZnP-phen=Re** and BIH in DMA [43]. The double asterisk indicates the higher excited state.

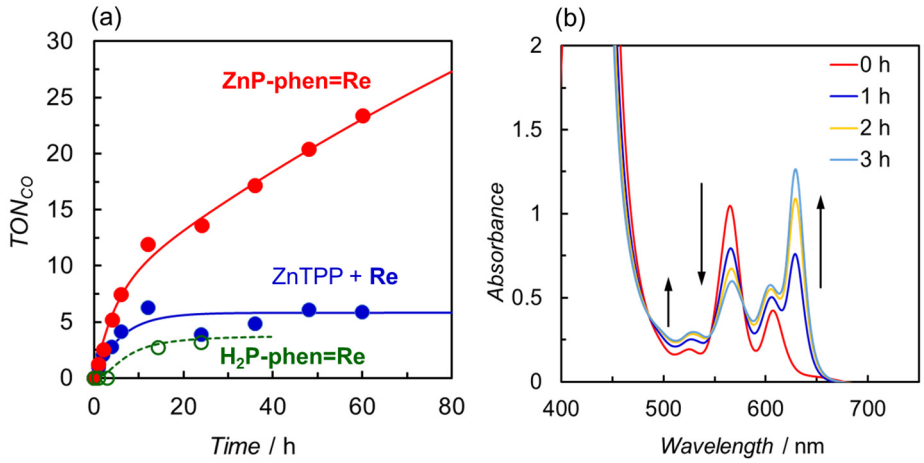

Figure 11. (**a**) Time dependences of CO formation during irradiation of CO_2-saturated DMA solutions containing TEA in the presence of **ZnP-phen=Re**, **H$_2$P-phen=Re**, or a mixed system of ZnTPP and *fac*-Re(phen)(CO)$_3$Br (**Re**) under irradiation at 420 nm. (**b**) UV–vis absorption spectral change in **ZnP-phen=Re** during the irradiation.

5. Special Pair Mimic Porphyrin Connected with Re Complex(es)

We reported porphyrin–Re complex systems that drive the photocatalytic CO_2 reduction by a different reaction mechanism from the T_1-mediated mechanism observed in the above dyad (Figure 12 left). The porphyrin parts are composed of a slipped-cofacial coordination dimer that is formed by the complementary coordination from the imidazolyl to the Zn ion [48,49]. The dimer mimics the special pair in the photosynthetic systems well. The dimer can delocalize a radical anion or cation over two porphyrins, which accelerates the CS rate in the photoinduced electron transfer and decelerates the charge recombination rate. Therefore, the dimer stabilizes the CS state [50,51]. In the porphyrin–Re complex systems shown in Figure 12 (left) the porphyrin units of the dimer are connected to each other through covalent bonds on the olefin moieties at the *meso*-positions of the porphyrin,

and the dimers have Re complex(es) on either one side (**ReD′**) or two sides (**ReD′Re**) via phenylene linker(s) [52].

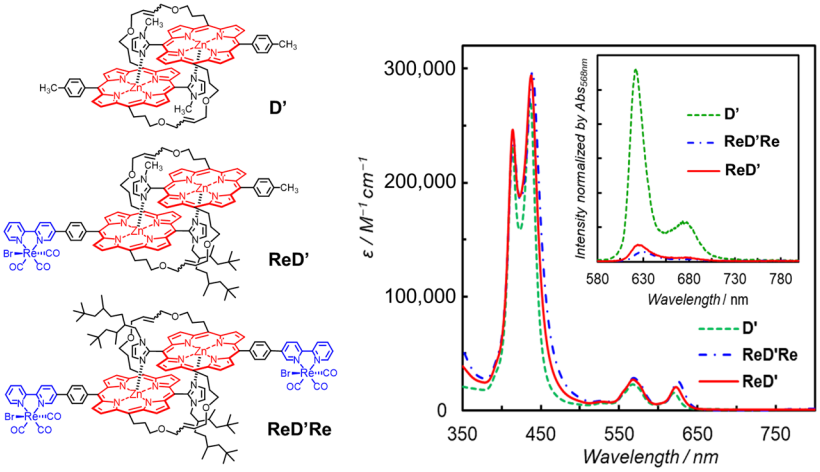

Figure 12. (**Left**) Chemical structures of the porphyrin dimers without (**D′**) and with the Re complex(es) (**ReD′Re** and **ReD′**). (**Right**) UV–vis absorption spectra of **D′**, **ReD′Re**, and **ReD′** in DMA. The inset presents fluorescence spectra of **D′**, **ReD′Re**, and **ReD′** in DMA at 298 K.

The UV–vis absorption spectra of **D′**, **ReD′Re**, and **ReD′** (Figure 12 right) showed that the Soret band split into two peaks due to strong exciton coupling between the two porphyrins in the dimer [49]. In contrast, the Q band was negligibly small due to the smaller oscillator strength. The broader Soret band caused by the exciton coupling enables the use of a very wide wavelength range of visible light for photocatalytic reactions. The fluorescence spectra of **ReD′Re**, and **ReD′** (Figure 12 right) were significantly quenched in polar DMA (dielectric constant: ε_s = 38.3) compared with **D′** and the fluorescence quenching was not observed in less-polar toluene (ε_s = 2.43), indicating that the intramolecular electron transfer from the S_1 of porphyrin dimer to the Re complex occurs in **ReD′Re** and **ReD′**. This behavior is in contrast to **ZnP-phen=Re**. In addition, no room-temperature phosphorescence was observed in **ReD′Re** and **ReD′**.

Photocatalytic CO_2 reduction was first carried out in a DMA solution containing **ReD′** using BIH as the electron donor by irradiating at 560 nm, but only a trace amount of CO was detected. The addition of TEOA dramatically increased CO production, whose TON_{CO} reached 2800 after 18 h without H_2 and formic acid formation (Figure 13). TEOA would contribute to assist trapping CO_2 by forming the Re(bpy)$(CO)_3$(CO_2-TEOA) species, facilitating the catalytic reaction on the Re complex [53]. The time profile for the reaction using **ReD′Re** was similar to that using **ReD′** in the same amount of CO production, indicating that the absorbed light energy can be used by one Re complex site for the CO_2 reduction reaction and that the catalytic activity of the Re complex is unaffected by the other Re complex. It is noted that obtaining the same amount of CO means that **ReD′Re**, which has two Re complex sites, is half that of **ReD′** when converted to TON_{CO} against the Re atom. The TON_{CO} of **ReD′** was an order of magnitude higher than the value (172 after 18 h) of **ZnP-phen=Re** under the optimal conditions (Figure 13). Herein, in **ZnP-phen=Re**, TEOA promoted the formation of chlorins and decreased the reaction rate, whereas in **ReD′Re** and **ReD** TEOA did not react with the porphyrin dimer.

The reaction quantum yields for **ReD′Re** and **ReD′** gave the same values of ca. 2% upon excitation to the S_2 of the porphyrin by λ_{ex} = 420 and 450 nm and to the S_1 by λ_{ex} = 560 nm. Considering that the reaction quantum yield of **ZnP-phen=Re** was 8% in DMA containing PhOH, these values were lower than expected and did not seem to reflect the reaction rate in Figure 13. We focused on the fact that the difference between the measurements of reaction quantum yield and TON_{CO} is the light irradiation intensity. Figure 14a shows the relationship between the reaction quantum yield and the irradiation light intensity at 560 nm for **ReD′** and **ZnP-phen=Re**. The reaction quantum yield of

ReD′ was independent of the light intensity, whereas that of **ZnP-phen=Re** significantly decreased as the light intensity increased. The decrease in the reaction quantum yield by increasing the irradiation light intensity would result from the accumulation of the OERS of porphyrin, which absorbs 560 nm light. This behavior is rather commonly observed in photocatalytic systems as the inner-filter effect caused by OERS absorption [54]. Figure 14b shows that the OERS of porphyrin accumulated during the irradiation in **ZnP-phen=Re**, whereas in **ReD′,** the OERS did not form during the irradiation. This spectral invariance would lead to the insensitivity of the reaction quantum yield to the irradiation light intensity. Therefore, even under excitation with intense light, the photocatalytic CO_2 reduction using **ReD′** proceeds without deactivation caused by the internal filter effect in which the OERS absorbs light, as observed in general photosensitizers. It is noteworthy that **ZnP-phen=Re** showed high durability even though the OERS of porphyrin accumulated. This indicates that the OERS of porphyrin is not a species that directly decomposes the photocatalyst.

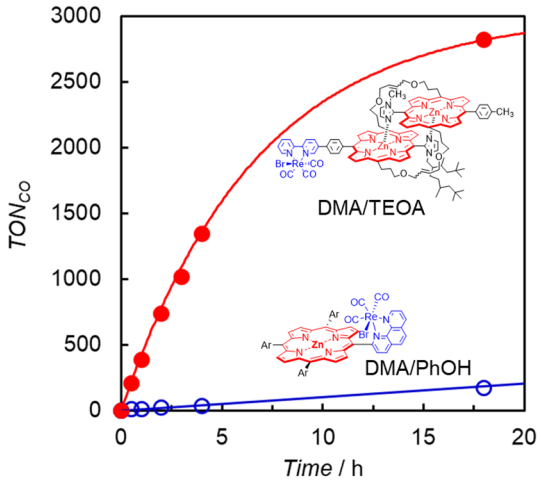

Figure 13. CO formation with time during irradiation at 560 nm from LED lamps for CO_2-saturated DMA solutions in the presence of BIH, containing either (red filled circle) **ReD′** with TEOA or (blue open circle) **ZnP-phen=Re** with PhOH.

To clarify whether the dimeric structure of the porphyrin contributes to the catalytic activity, photocatalytic CO_2 reductions were carried out under the same conditions in a coordination solvent of dimethyl sulfoxide (DMSO) using **ReD′Re** and **ReDRe** in which the porphyrin units of the dimer are "not" connected to each other through covalent bonds on the olefin moieties at the *meso*-positions of the porphyrin. In DMSO, **ReDRe** dissociated into the DMSO-coordinated monomer under micromolar-order concentration conditions. Figure 15 shows the time profile of CO production upon excitation at the Q band, which is similar between the monomer and dimer. In **ReD′Re**, the TON_{CO} reached 1800 (based on the Re atom), which was much larger than in the system using the porphyrin monomer (**ReDRe**). The UV–vis spectral changes during irradiation show that the spectrum of **ReD′Re** hardly changed, as observed at the bottom of Figure 14b, but the spectrum of the monomer significantly decreased by the hydrogenation of the porphyrin. The dimer is superior to the monomer in durability. BIH produces a very strong reductant, $BI^{\bullet}$ [18], and the two-electron-reduced species on the porphyrin unit can be generated. Even when the two-electron-reduced porphyrin is formed, the dimeric structure can share electrons between the two porphyrins of the dimer, suppressing the hydrogenation of the porphyrin.

A plausible reaction diagram is shown in Figure 16. The porphyrin dimer can absorb a wide wavelength range of visible light to give the S_1 of porphyrin. The fluorescence quenching showed that efficient intramolecular electron transfer occurred to give the CS state, which is stabilized with the dimeric structure. Because a rapid back-electron-transfer process from the CS to the ground state should compete with the catalytic reaction, the addition of TEOA, which assists the formation of CO_2 adduct with the Re complex and

promotes the following subsequent reaction after reduction of the Re complex, would be essential. With the assistance of TEOA, the transient-reduced Re complex would rapidly react with CO_2 to afford a more stable reaction intermediate that suppresses the back-electron transfer. In this mechanism, BIH neutralizes the cation radical of the porphyrin to give the ground state porphyrin, and no long-lived OERS of porphyrin is formed. The above results indicate that **ReD′** (**ReD′Re**) proceeds by a different mechanism from that of **ZnP-phen=Re** and shows an extremely high activity under irradiation with intense light.

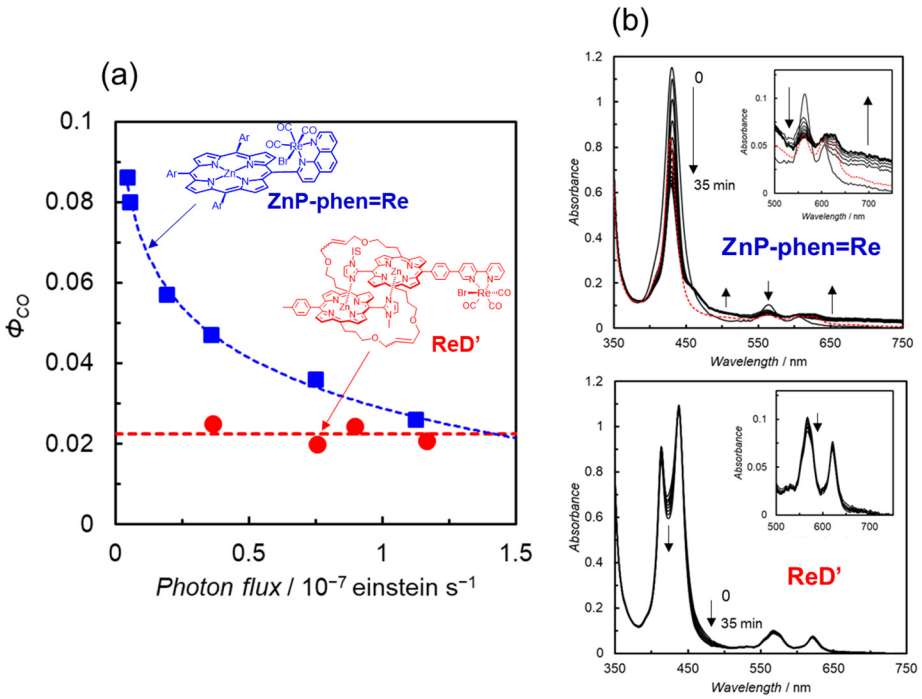

Figure 14. (**a**) Relationship between the reaction quantum yield and the irradiation light intensity at 560 nm in CO_2-saturated DMA solutions containing BIH for (red circle) **ReD′** with TEOA and (blue square) **ZnP-phen=Re** with PhOH. (**b**) UV–vis absorption spectral changes in **ZnP-phen=Re** (5.0 μM) and **ReD′** (2.5 μM) during the irradiation at 560 nm (0.35×10^{-7} einstein s^{-1}). Red dotted lines show the spectra of resulting solutions after standing for 2 d in the dark.

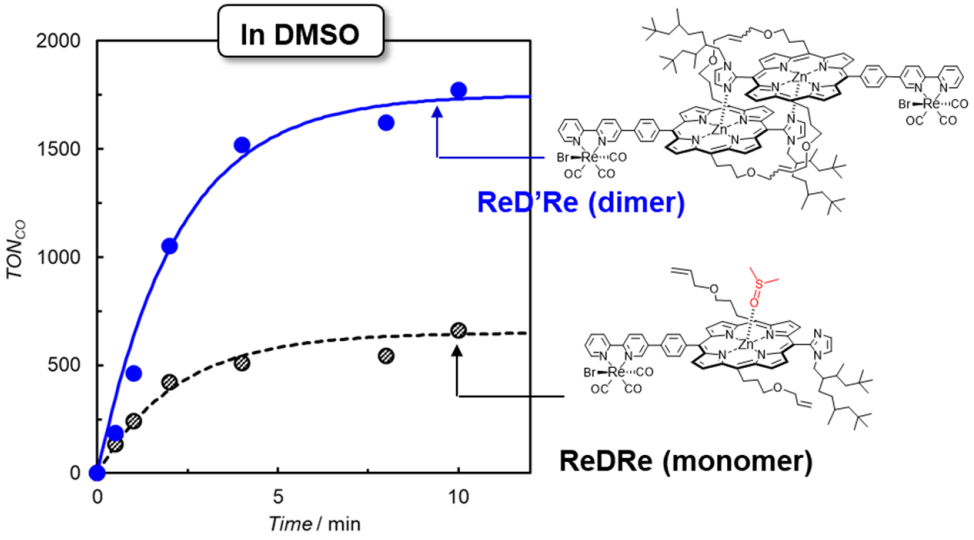

Figure 15. CO formation with time during irradiation at 560 nm from LED lamps for CO_2-saturated DMSO–TEOA solutions containing **ReD′Re** (2.5 μM) and **ReDRe** (2.5 μM) in the presence of BIH (0.01 M, 2000 equiv against the Re complex). The TON_{CO} is calculated against the Re atom.

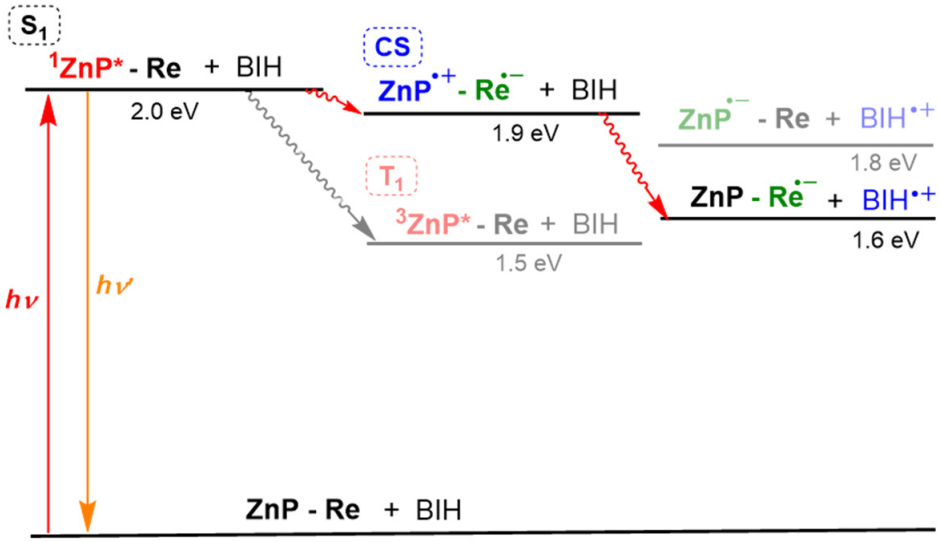

Figure 16. An energy diagram of **ReD′** and BIH in DMA–TEOA. The "**Re**" corresponds to the TEOA-CO_2 adduct, which can change into a more stable reaction intermediate after reduction by the intramolecular electron transfer.

6. Conclusions

In the photocatalytic CO_2 reduction, Zn porphyrins are hydrogenated and bleached during the irradiation, and the catalytic reaction is stopped. The durability of Zn porphyrins is improved by suppressing the accumulation of more than two electrons on the Zn porphyrins. We designed two types of Zn porphyrin–Re complex systems, **ZnP-phen=Re** and **ReD′** (**ReD′Re**). In **ZnP-phen=Re**, the photocatalytic CO_2 reduction proceeds via the initial electron transfer from BIH to the long-lived T_1. Further electron accumulation in the OERS of the porphyrin would be suppressed by the rapid electron transfer to the Re complex. The efficient initial electron transfer via the T_1 achieves the high reaction quantum yield (8%) of CO production. In **ReD′** (**ReD′Re**), the reaction mechanism via the CS state does not give the long-lived OERS of porphyrin, so no species that inhibits light absorption is accumulated. Therefore, the high TON_{CO} reaching 2800 for **ReD′** under irradiation of relatively intense light at 560 nm can be achieved. However, in **ReD′** (**ReD′Re**), the competitive back-electron transfer from the CS to the ground state limits the reaction quantum yield to 2%. Both systems have advantages and disadvantages, and it is necessary to elucidate the reaction mechanism in detail by time-resolved measurements and to develop better photocatalysts by improving the molecular design based on the mechanism.

This paper did not describe the second electron required for the CO_2 reduction reaction. The second reduction process is important for a better understanding of the reaction mechanism. However, this process is thought to be much faster than the initial process. So far, the second reduction process has not been directly observed even in the mononuclear Re complex or the Ru–Re complex systems [55,56]. To observe the second reduction process, new measurement methodologies and instruments are required.

Author Contributions: Conceptualization, Y.K.; writing—original draft preparation, Y.K.; writing—review and editing, A.S.; project administration, Y.K. and A.S.; funding acquisition, Y.K. All authors have read and agreed to the published version of the manuscript.

Funding: This work was funded by JSPS KAKENHI grant number JP22H02186 and the Carbon Recycling Fund Institute of Japan.

Data Availability Statement: No new data were created or analyzed in this study. Data sharing is not applicable to this article. Refer to the original papers for data availability.

Conflicts of Interest: The authors declare no conflict of interest.

References

1. Friedlingstein, P.; O'Sullivan, M.; Jones, M.W.; Andrew, R.M.; Gregor, L.; Hauck, J.; Le Quéré, C.; Luijkx, I.T.; Olsen, A.; Peters, G.P.; et al. Global carbon budget 2022. *Earth Syst. Sci. Data* **2022**, *14*, 4811–4900. [CrossRef]
2. Kuramochi, Y.; Ishitani, O.; Ishida, H. Reaction mechanisms of catalytic photochemical CO_2 reduction using Re(I) and Ru(II) complexes. *Coord. Chem. Rev.* **2018**, *373*, 333–356. [CrossRef]
3. Yamazaki, Y.; Takeda, H.; Ishitani, O. Photocatalytic reduction of CO_2 using metal complexes. *J. Photochem. Photobiol. C* **2015**, *25*, 106–137. [CrossRef]
4. Elgrishi, N.; Chambers, M.B.; Wang, X.; Fontecave, M. Molecular polypyridine-based metal complexes as catalysts for the reduction of CO_2. *Chem. Soc. Rev.* **2017**, *46*, 761–796. [CrossRef]
5. Luo, Y.-H.; Dong, L.-Z.; Liu, J.; Li, S.-L.; Lan, Y.Q. From molecular metal complex to metal-organic framework: The CO_2 reduction photocatalysts with clear and tunable structure. *Coord. Chem. Rev.* **2019**, *390*, 86–126. [CrossRef]
6. Nakada, A.; Kumagai, H.; Robert, M.; Ishitani, O.; Maeda, K. Molecule/Semiconductor Hybrid Materials for Visible-Light CO_2 Reduction: Design Principles and Interfacial Engineering. *Acc. Mater. Res.* **2021**, *2*, 458–470. [CrossRef]
7. Son, H.-J.; Pac, C.; Kang, S.O. Inorganometallic Photocatalyst for CO_2 Reduction. *Acc. Chem. Res.* **2021**, *54*, 4530–4544. [CrossRef]
8. Pirzada, B.M.; Dar, A.H.; Shaikh, M.N.; Qurashi, A. Reticular-Chemistry-Inspired Supramolecule Design as a Tool to Achieve Efficient Photocatalysts for CO_2 Reduction. *ACS Omega* **2021**, *6*, 29291–29324. [CrossRef]
9. Fujita, E.; Grills, D.C.; Manbeck, G.F.; Polyansky, D.E. Understanding the Role of Inter- and Intramolecular Promoters in Electro- and Photochemical CO_2 Reduction Using Mn, Re, and Ru Catalysts. *Acc. Chem. Res.* **2022**, *55*, 616–628. [CrossRef]
10. Bizzarri, C. Homogeneous Systems Containing Earth-Abundant Metal Complexes for Photoactivated CO_2 Reduction: Recent Advances. *Eur. J. Org. Chem.* **2022**, *24*, e202200185.
11. Rudolph, M.; Dautz, S.; Jäger, E.-G. Macrocyclic [N_4^{2-}] Coordinated Nickel Complexes as Catalysts for the Formation of Oxalate by Electrochemical Reduction of Carbon Dioxide. *J. Am. Chem. Soc.* **2000**, *122*, 10821–10830. [CrossRef]
12. Rao, H.; Schmidt, L.C.; Bonin, J.; Robert, M. Visible-light-driven methane formation from CO_2 with a molecular iron catalyst. *Nature* **2017**, *548*, 74–77. [CrossRef]
13. Sato, S.; Arai, T.; Morikawa, T.; Uemura, K.; Suzuki, T.M.; Tanaka, H.; Kajino, T. Selective CO_2 conversion to formate conjugated with H_2O oxidation utilizing semiconductor/complex hybrid photocatalysts. *J. Am. Chem. Soc.* **2011**, *133*, 15240–15243. [CrossRef]
14. Sahara, G.; Kumagai, H.; Maeda, K.; Kaeffer, N.; Artero, V.; Higashi, M.; Abe, R.; Ishitani, O. Photoelectrochemical reduction of CO_2 Coupled to water oxidation using a photocathode with a Ru(II)–Re (I) complex photocatalyst and a CoO_x/TaON photoanode. *J. Am. Chem. Soc.* **2016**, *138*, 14152–14158. [CrossRef]
15. Suzuki, T.M.; Yoshino, S.; Takayama, T.; Iwase, A.; Kudo, A.; Morikawa, T. Z-Schematic and visible-light-driven CO_2 reduction using H_2O as an electron donor by a particulate mixture of a Ru complex/$(CuGa)_{1-x}Zn_{2x}S_2$ hybrid catalyst, $BiVO_4$ and an electron mediator. *Chem. Commun.* **2018**, *54*, 10199–10202. [CrossRef]
16. Kamata, R.; Kumagai, H.; Yamazaki, Y.; Sahara, G.; Ishitani, O. Photoelectrochemical CO_2 reduction using a Ru(II)-Re(I) supramolecular photocatalyst connected to a vinyl polymer on a NiO electrode. *ACS Appl. Mater. Interfaces* **2019**, *11*, 5632–5641. [CrossRef]
17. Tamaki, Y.; Ishitani, O. Supramolecular photocatalysts for the reduction of CO_2. *ACS Catal.* **2017**, *7*, 3394–3409. [CrossRef]
18. Tamaki, Y.; Koike, K.; Morimoto, T.; Ishitani, O. Substantial improvement in the efficiency and durability of a photocatalyst for carbon dioxide reduction using a benzoimidazole derivative as an electron donor. *J. Catal.* **2013**, *304*, 22–28. [CrossRef]
19. Kuttassery, F.; Kumagai, H.; Kamata, R.; Ebato, Y.; Higashi, M.; Suzuki, H.; Abe, R.; Ishitani, O. Supramolecular photocatalysts fixed on the inside of the polypyrrole layer in dye sensitized molecular photocathodes: Application to photocatalytic CO_2 reduction coupled with water oxidation. *Chem. Sci.* **2021**, *12*, 13216–13232. [CrossRef]
20. Taniguchi, M.; Lindsey, J.S. Synthetic chlorins, possible surrogates for chlorophylls, prepared by derivatization of porphyrins. *Chem. Rev.* **2017**, *117*, 344–535. [CrossRef]
21. Otsuki, J. Supramolecular approach towards light-harvesting materials based on porphyrins and chlorophylls. *J. Mater. Chem. A* **2018**, *6*, 6710–6753. [CrossRef]
22. Nagata, N.; Kuramochi, Y.; Kobuke, Y. Energy transfer among light-harvesting macrorings incorporated into a bilayer membrane. *J. Am. Chem. Soc.* **2009**, *131*, 10–11. [CrossRef]
23. Kuramochi, Y.; Sandanayaka, A.S.D.; Satake, A.; Araki, Y.; Ogawa, K.; Ito, O.; Kobuke, Y. Energy transfer followed by electron transfer in a porphyrin macrocycle and central acceptor ligand: A model for a photosynthetic composite of the light-harvesting complex and reaction center. *Chem.-Eur. J.* **2009**, *15*, 2317–2327. [CrossRef]
24. Kuramochi, Y.; Satake, A.; Kobuke, Y. Light harvesting macroring accommodating a tetrapodal ligand based on complementary and cooperative coordinations. *J. Am. Chem. Soc.* **2004**, *126*, 8668–8669. [CrossRef]
25. Borah, K.D.; Bhuyan, J. Magnesium porphyrins with relevance to chlorophylls. *Dalton Trans.* **2017**, *46*, 6497–6509. [CrossRef]
26. Chen, L.X.; Zhang, X.; Wasinger, E.C.; Attenkofer, K.; Jennings, G.; Muresan, A.Z.; Lindsey, J.S. Tracking Electrons and Atoms in a Photoexcited Metalloporphyrin by X-ray Transient Absorption Spectroscopy. *J. Am. Chem. Soc.* **2007**, *129*, 9616–9618. [CrossRef]
27. Nikoloudakis, E.; López-Duarte, I.; Charalambidis, G.; Ladomenou, K.; Ince, M.; Coutsolelos, A.G. Porphyrins and phthalocyanines as biomimetic tools for photocatalytic H_2 production and CO_2 reduction. *Chem. Soc. Rev.* **2022**, *51*, 6965–7045. [CrossRef]

28. Kiyosawa, K.; Shiraishi, N.; Shimada, T.; Masui, D.; Tachibana, H.; Takagi, S.; Ishitani, O.; Tryk, D.A.; Inoue, H. Electron transfer from the porphyrin S_2 State in a zinc porphyrin-rhenium bipyridyl dyad having carbon dioxide reduction activity. *J. Phys. Chem. C* **2009**, *113*, 11667–11673. [CrossRef]
29. Schneider, J.; Vuong, K.Q.; Calladine, J.A.; Sun, X.-Z.; Whitwood, A.C.; George, M.W.; Perutz, R.N. Photochemistry and photophysics of a Pd(II) metalloporphyrin: Re(I) tricarbonyl bipyridine molecular dyad and its activity toward the photoreduction of CO_2 to CO. *Inorg. Chem.* **2011**, *50*, 11877–11889. [CrossRef]
30. Windle, C.D.; Campian, M.V.; Duhme-Klair, A.-K.; Gibson, E.A.; Perutz, R.N.; Schneider, J. CO_2 photoreduction with long-wavelength light: Dyads and monomers of zinc porphyrin and rhenium bipyridine. *Chem. Commun.* **2012**, *48*, 8189–8191. [CrossRef]
31. Windle, C.D.; George, M.W.; Perutz, R.N.; Summers, P.A.; Sun, X.Z.; Whitwood, A.C. Comparison of rhenium–porphyrin dyads for CO_2 photoreduction: Photocatalytic studies and charge separation dynamics studied by time-resolved IR spectroscopy. *Chem. Sci.* **2015**, *6*, 6847–6864. [CrossRef] [PubMed]
32. Kitagawa, Y.; Takeda, H.; Ohashi, K.; Asatani, T.; Kosumi, D.; Hashimoto, H.; Ishitani, O.; Tamiaki, H. Photochemical reduction of CO_2 with red light using synthetic chlorophyll–rhenium bipyridine dyad. *Chem. Lett.* **2014**, *43*, 1383–1385. [CrossRef]
33. Matlachowski, C.; Braun, B.; Tschierlei, S.; Schwalbe, M. Photochemical CO_2 reduction catalyzed by phenanthroline extended tetramesityl porphyrin complexes linked with a rhenium-(I) tricarbonyl unit. *Inorg. Chem.* **2015**, *54*, 10351–10360. [CrossRef]
34. Lang, P.; Pfrunder, M.; Quach, G.; Braun-Cula, B.; Moore, E.G.; Schwalbe, M. Sensitized photochemical CO_2 reduction by hetero–Pacman compounds linking a ReI tricarbonyl with a porphyrin unit. *Chem.-Eur. J.* **2019**, *25*, 4509–4519. [CrossRef] [PubMed]
35. Kuramochi, Y.; Fukaya, K.; Yoshida, M.; Ishida, H. Trans-(Cl)-[Ru(5,5′-diamide-2,2′-bipyridine)$(CO)_2Cl_2$]: Synthesis, structure, and photocatalytic CO_2 reduction activity. *Chem.-Eur. J.* **2015**, *21*, 10049–10060. [CrossRef]
36. Gabrielsson, A.; Lindsay Smith, J.R.; Perutz, R.N. Remote site photosubstitution in metalloporphyrin–rhenium tricarbonylbipyridine assemblies: Photo-reactions of molecules with very short lived excited states. *Dalton Trans.* **2008**, 4259–4269. [CrossRef]
37. Gabrielsson, A.; Hartl, F.; Zhang, H.; Lindsay Smith, J.R.; Towrie, M.; Vlcek, A.; Perutz, R.N. Ultrafast charge separation in a photoreactive rhenium-appended porphyrin assembly monitored by picosecond transient infrared spectroscopy. *J. Am. Chem. Soc.* **2006**, *128*, 4253–4266. [CrossRef]
38. Koike, K.; Hori, H.; Ishizuka, M.; Westwell, J.R.; Takeuchi, K.; Ibusuki, T.; Enjouji, K.; Konno, H.; Sakamoto, K.; Ishitani, O. Key process of the photocatalytic reduction of CO_2 using [Re(4,4′-X_2-bipyridine)$(CO)_3PR_3]^+$ (X = CH_3, H, CF_3; PR_3 = phosphorus ligands): Dark reaction of the one-electron-reduced complexes with CO_2. *Organometallics* **1997**, *16*, 5724–5729. [CrossRef]
39. Lanese, J.G.; Wilson, G.S. Electrochemical studies of zinc tetraphenylporphin. *J. Electrochem. Soc.* **1972**, *119*, 1039–1043. [CrossRef]
40. Yamaguchi, H.; Soeta, A.; Toeda, H.; Itoh, K. Raman scattering study on electrochemical reduction products of magnesium, zinc and copper tetraphenylporphines. *J. Electroanal. Chem. Interfacial Electrochem.* **1983**, *159*, 347–359. [CrossRef]
41. Closs, G.L.; Closs, L.E. Negative ions of porphin metal complexes. *J. Am. Chem. Soc.* **1963**, *85*, 818–819. [CrossRef]
42. Whitlock, H.W.; Oester, M.Y. Behavior of di- and tetrahydroporphyrins under alkaline conditions. Direct observation of the chlorin-phlorin equilibrium. *J. Am. Chem. Soc.* **1973**, *95*, 5738–5741. [CrossRef] [PubMed]
43. Kuramochi, Y.; Fujisawa, Y.; Satake, A. Photocatalytic CO_2 reduction mediated by electron transfer via the excited triplet state of Zn(II) porphyrin. *J. Am. Chem. Soc.* **2020**, *142*, 705–709. [CrossRef]
44. Kuramochi, Y.; Satake, A. Photocatalytic CO_2 reductions catalyzed by meso-(1,10-Phenanthrolin-2-yl)-porphyrins having a rhenium(I) tricarbonyl complex. *Chem.-Eur. J.* **2020**, *26*, 16365–16373. [CrossRef]
45. Kuramochi, Y.; Kamiya, M.; Ishida, H. Photocatalytic CO_2 reduction in *N*,*N*-dimethylacetamide/water as an alternative solvent system. *Inorg. Chem.* **2014**, *53*, 3326–3332. [CrossRef] [PubMed]
46. Quimby, D.J.; Longo, F.R. Luminescence studies on several tetraarylporphins and their zinc derivatives. *J. Am. Chem. Soc.* **1975**, *97*, 5111–5117. [CrossRef]
47. Smieja, J.M.; Benson, E.E.; Kumar, B.; Grice, K.A.; Seu, C.S.; Miller, A.J.M.; Mayer, J.M.; Kubiak, C.P. Kinetic and structural studies, origins of selectivity, and interfacial charge transfer in the artificial photosynthesis of CO. *Proc. Natl. Acad. Sci. USA* **2012**, *109*, 15646–15650. [CrossRef]
48. Kobuke, Y.; Miyaji, H. Supramolecular organization of imidazolyl-porphyrin to a slipped cofacial dimer. *J. Am. Chem. Soc.* **1994**, *116*, 4111–4112. [CrossRef]
49. Satake, A.; Kobuke, Y. Artificial photosynthetic systems: Assemblies of slipped cofacial porphyrins and phthalocyanines showing strong electronic coupling. *Org. Biomol. Chem.* **2007**, *5*, 1679–1691. [CrossRef]
50. Ozeki, H.; Nomoto, A.; Ogawa, K.; Kobuke, Y.; Murakami, M.; Hosoda, K.; Ohtani, M.; Nakashima, S.; Miyasaka, H.; Okada, T. Role of the special pair in the charge-separating event in photosynthesis. *Chem.-Eur. J.* **2004**, *10*, 6393–6401. [CrossRef]
51. Ito, F.; Ishibashi, Y.; Khan, S.R.; Miyasaka, H.; Kameyama, K.; Morisue, M.; Satake, A.; Ogawa, K.; Kobuke, Y. Photoinduced electron transfer and excitation energy transfer in directly linked zinc porphyrin/zinc phthalocyanine composite. *J. Phys. Chem. A* **2006**, *110*, 12734–12742. [CrossRef] [PubMed]
52. Kuramochi, Y.; Sato, R.; Sakuma, H.; Satake, A. Photocatalytic CO_2 reduction sensitized by a special-pair mimic porphyrin connected with a rhenium(i) tricarbonyl complex. *Chem. Sci.* **2022**, *13*, 9861–9879. [CrossRef]
53. Morimoto, T.; Nakajima, T.; Sawa, S.; Nakanishi, R.; Imori, D.; Ishitani, O. CO_2 capture by a rhenium(I) complex with the aid of triethanolamine. *J. Am. Chem. Soc.* **2013**, *135*, 16825–16828. [CrossRef] [PubMed]

54. Takeda, H.; Koike, K.; Inoue, H.; Ishitani, O. Development of an efficient photocatalytic system for CO_2 reduction using rhenium(I) complexes based on mechanistic studies. *J. Am. Chem. Soc.* **2008**, *130*, 2023–2203. [CrossRef] [PubMed]
55. Kou, Y.; Nabetani, Y.; Nakazato, R.; Pratheesh, N.V.; Sato, T.; Nozawa, S.; Adachi, S.; Tachibana, H.; Inoue, H. Mechanism of the photoreduction of carbon dioxide catalyzed by the benchmarking rhenium dimethylbipyridine complexes; Operando measurements by XAFS and FT-IR. *J. Catal.* **2022**, *405*, 508–519. [CrossRef]
56. Kamogawa, K.; Shimoda, Y.; Miyata, K.; Onda, K.; Yamazaki, Y.; Tamaki, Y.; Ishitani, O. Mechanistic study of photocatalytic CO_2 reduction using a Ru(II)-Re(I) supramolecular photocatalyst. *Chem. Sci.* **2021**, *12*, 9682–9693. [CrossRef]